THE JOURNAL OF PHYSICAL CHEMISTRY C

Article

Cite This: J. Phys. Chem. C 2018, 122, 29307−29318

pubs.acs.org/JPCC

Theoretical Approaches to Describing the Oxygen Reduction Reaction Activity of Single-Atom Catalysts

Anjli M. Patel,[†] Stefan Ringe,[†] Samira Siahrostami,[†] Michal Bajdich,[‡] Jens K. Nørskov,*[,∥] and Ambarish R. Kulkarni*[,§]

[†]SUNCAT Center for Interface Science and Catalysis, Department of Chemical Engineering, Stanford University, Stanford 94305, California, United States

[‡]SUNCAT Center for Interface Science and Catalysis, SLAC National Accelerator Laboratory, 2575 Sand Hill Road, Menlo Park, California 94025, United States

[§]Department of Chemical Engineering, University of California, Davis, Davis 95616, California, United States

[∥]Department of Physics, Technical University of Denmark, Lyngby 2800 Kgs, Denmark

Supporting Information

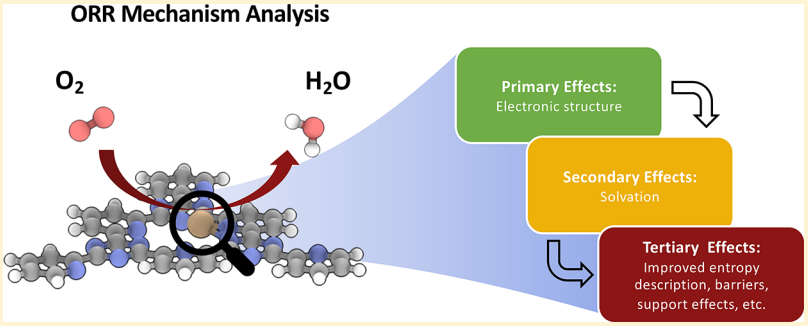

ABSTRACT: Single-atom catalysts have recently emerged as promising low-cost alternatives to Pt for the oxygen reduction reaction (ORR). Given the unique properties that distinguish these systems from traditional transition-metal electrocatalysts, it is essential to benchmark and establish appropriate computational approaches to study these novel materials. Herein, we employ multiple levels of theory, including wave function methods, density functional theory (DFT), and classical simulations, to investigate Cu-modified covalent triazine framework catalysts (Cu/CTF). We consider three major aspects of treating this system computationally. First, we present a step-wise approach to predict the ORR mechanism and adsorbate coverages on Cu/CTF. We then benchmark various DFT methods to coupled-cluster theory with the domain-based local pair natural orbital approximation, which indicates that HSE06 and PBE0 hybrid functionals most accurately describe the adsorption energies of ORR adsorbates on Cu/CTF. We finally employ thermodynamic integration and other techniques to consider solvation effects, which play significant roles in predicting the energies of reaction intermediates and the overall ORR pathway. Our findings indicate that accurate descriptions of both the electronic structure and solvation are necessary to understand the ORR activity of Cu/CTF.

1. INTRODUCTION

The oxygen reduction reaction (ORR) plays a critical role in advanced energy conversion technologies, including polymer exchange membrane fuel cells and metal−air batteries. The efficiency of these devices is often limited by sluggish ORR kinetics, and the most active and widely used electrocatalysts rely on expensive platinum-based alloys.[1] The scaling between *OOH and *OH limits the theoretical overpotential for these electrocatalysts to approximately 0.4 V_{RHE}.[2,3] As a result, significant research efforts have been devoted to developing less expensive alternatives by using non-precious materials.[4−6] It has also been suggested that the limitations in the activity of current catalysts are due to the scaling relations between the reaction intermediates.[2,7] Finding ways to design new types of active sites that circumvent these scaling relations has been suggested to be a high priority target.[7,8]

Motivated by the potential of single-atom catalysts to match or surpass the activity of platinum,[9−17] considerable experimental and computational work has been focused on exploring these materials for ORR. These classes of materials exhibit unique structures and properties that can potentially compete with platinum by allowing the use of abundant and inexpensive active site elements without compromising the catalytic activity. For example, a variety of M−N−C catalysts, such as FeN_4 in

Received: September 27, 2018
Revised: November 21, 2018
Published: November 29, 2018

DOI: 10.1021/acs.jpcc.8b09430
J. Phys. Chem. C 2018, 122, 29307−29318

graphene,[18] Co/C_3N_4,[19,20] and Ru-modified nitrogen-doped graphene,[21] have shown encouraging ORR performance.

Previous theoretical studies on M−N−C materials[22−25] have largely applied computational protocols originally developed for transition-metal surfaces.[2,26,27] For instance, transition metals are often described using periodic density functional theory (DFT) with generalized gradient approximation (GGA) functionals, which have been useful for screening the activity of single-atom materials. The accuracy of these computational methods has been well-established for metals,[28−30] but it is unclear whether these methods are directly transferable to single-atom catalysts. Given the increasing popularity of theory-driven approaches for designing novel single-atom catalysts, it is important to develop and implement computational methods that accurately describe the complexity of these systems. Herein, we demonstrate a multiscale modeling strategy by studying one particular single-atom catalyst, copper-modified covalent triazine frameworks (Cu/CTF).

Covalent triazine frameworks are amorphous porous organic polymers consisting of triazine-linked monomeric units.[31,32] Recent experimental work from Kamiya et al. shows that incorporating single-atom active sites, such as Pt or Cu, into these systems results in enhanced ORR activity.[33,34] Based on extended X-ray absorption fine structure measurements, this improvement in activity is attributed to the single-atom nature of the active site. The ORR overpotential of this system in a neutral electrolyte is approximately 0.2 V_{RHE} greater than platinum on carbon (Pt/C).[33] More recently, the authors improved the activity of Cu/CTF by tuning the coordination environment of Cu (Cu−S−CTF).[35]

Given the multitude of factors that may affect reactivity (e.g. adsorbate coverages, binding energies, solvation effects, anharmonic entropic contributions, etc.), it is useful to delineate these contributions into primary, secondary, and tertiary effects. Broadly, these contributions are ordered based on dependency and increasing computational cost necessary to correctly incorporate these effects. Primary effects include choosing an appropriate electronic structure method to calculate the energetics and potential-dependent coverages of relevant reaction intermediates. As the CTF structure is composed of distinct monomeric units (Figure 1a), we use truncated cluster models and the coupled-cluster approach with the domain-based local pair natural orbital (DLPNO) approximation to benchmark various DFT functionals (Results and Discussion Section 3.2). After identifying an appropriate DFT functional, we include the secondary solvation effects using thermodynamic integration (TI) based on a DFT-derived classical force field in Section 3.3. Our results indicate that considering these two aspects enables theoretical simulations to describe ORR activity trends on metal-modified CTF materials. This knowledge may be valuable for large-scale electrocatalyst optimization and exploration.

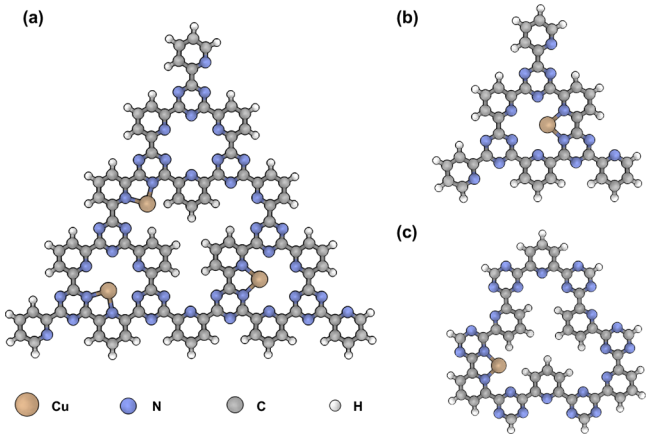

Figure 1. Chemical structures of (a) Cu/CTF, (b) Cu/CTF(6N), and (c) Cu/CTF(9N) models.

2. COMPUTATIONAL METHODS

2.1. Periodic DFT. The Vienna ab initio simulation package (VASP)[36,37] was used to apply the Bayesian error estimation functional with van der Waals correlation (BEEF-vdW),[28] Perdew−Burke−Ernzerhof (PBE),[38,39] and revised PBE (RPBE) GGA functionals and the PBE0,[40] B3LYP,[41] and HSE06[42,43] hybrid functionals to model Cu/CTF and truncated Cu-based clusters. These systems were modeled using a plane wave cut-off energy of 400 eV, 1 × 1 × 1 *k*-points, and projector augmented wave (PAW) method pseudopotentials. The energy convergence limit was 10^{-5} eV/atom, and the force convergence criterion was 0.03 eV/Å for optimized structures. Using the DFT-D3 method with Becke−Johnson (BJ) damping,[44−46] dispersion corrections were added to all hybrid and GGA functional calculations except for BEEF−vdW, which inherently accounts for vdW interactions.[28]

2.2. DLPNO-CCSD(T) Benchmarking. For the Cu/2-phen system, single-point DLPNO-CCSD(T) calculations were executed on B3LYP-optimized geometries using the ORCA 4.0 quantum chemistry package.[47,48] The unrestricted Hartree−Fock reference was used for self-consistent field convergence, and quasi-restricted orbitals were subsequently used to calculate excitations.[49,50] The geometries of these systems were optimized with the B3LYP functional and the correlation consistent aug-cc-pVDZ basis set[51−53] while constraining framework atoms to avoid significant structural distortion. All calculations were performed at neutral charge. The electronic energies of the 2-phen clusters were extrapolated to the complete basis set limit using the second and third cardinal numbers for the augmented correlation consistent basis set (aug-cc-pVDZ and aug-cc-pVTZ) with the frozen core approximation. The geometries of the 2-phen and CTF systems were fixed for benchmarking studies to decouple geometry changes and differences in the description of the electronic structure by each method. In order to benchmark periodic DFT calculations in VASP with quantum chemical DLPNO-CCSD(T) calculations in ORCA, we established agreement between periodic and quantum chemical DFT in Figure S1.

2.3. Classical Monte Carlo Simulations. We used the RASPA software package[54] to conduct Monte Carlo (MC) simulations with the *NVT* ensemble at 300 K. The Cu/CTF system was modeled by a generic UFF/TraPPE force field prior to fitting, and we employed a modified TIP4P-Ew water model that reflected the geometry of water described by the RPBE functional. The purpose of modifying the water model geometry was to avoid fictitious forces in single-point RPBE-D3(BJ) DFT simulations of configurations obtained by classical MC simulations for the cluster-continuum solvation approach. The modified TIP4P-Ew geometry did not significantly impact predicted solvation energies. Our MC simulations included sufficient explicit water molecules to mimic the density of bulk liquid water, which corresponds to 417 water molecules for the CTF(6N) active site and 383 molecules for the CTF(3N) site. TI simulations were conducted by performing five parallel MC

DOI: 10.1021/acs.jpcc.8b09430
J. Phys. Chem. C 2018, 122, 29307−29318

simulations with 100 000 initialization cycles followed by 100 000 production run cycles. The final solvation free energies were computed by averaging the results of the five replicates.

In this study, the solvation free energy was calculated for each ORR adsorbate on Cu/CTF by separately removing electrostatic and vdW interactions between the adsorbate/framework system and surrounding water molecules to avoid numerical instabilities in the MC simulations. In each case, λ was varied from 0 to 1 in increments of 0.1. Coulombic interactions were scaled linearly with respect to λ. Unlike the Coulomb potential, the Lennard-Jones (LJ) potential used to scale vdW interactions encounters well-documented numerical instabilities when λ approaches zero.[55] While soft-core LJ potentials are often employed to address this issue in molecular dynamics (MD) simulations, numerical instabilities can be avoided in MC simulations through a change of variables in TI.[55−58] We performed this change of variables by conducting TI of vdW interactions with respect to λ^m, where $m = 0.25$ in accordance to the procedure introduced by Mruzik et al.[56]

3. RESULTS AND DISCUSSION

3.1. ORR Mechanism Analysis. Two pathways are commonly considered for ORR.[2] The first is the associative mechanism, which involves four proton−electron transfer steps shown in steps 1 through 4. The second ORR pathway is the dissociative mechanism, where O_2 dissociatively adsorbs to the catalyst surface according to step 5 and subsequently undergoes steps 3 and 4. The associative mechanism dominates at realistic potentials for commonly studied active ORR catalysts such as Pt(111),[2] and it is a likely pathway for Cu/CTF due to the single-atom nature of the active site.

$$O_2 + * + H^+ + e^- \rightleftharpoons *OOH \quad (1)$$

$$*OOH + H^+ + e^- \rightleftharpoons *O + H_2O \quad (2)$$

$$*O + H^+ + e^- \rightleftharpoons *OH \quad (3)$$

$$*OH + H^+ + e^- \rightleftharpoons H_2O \quad (4)$$

$$O_2 \rightleftharpoons 2*O \quad (5)$$

Similar to previous studies, we used the computational hydrogen electrode to describe the potential dependence of the reactions.[2] Electronic energies (using H_2O and H_2 as gas phase references) were converted to free energies by adding the zero point energy and entropy contributions using the harmonic approximation (Table S1). The applicability of the harmonic approximation and other potential tertiary effects are discussed in Section 3.4.

In addition to the "standard" methodology described above, we must consider additional effects to account for the single-atom nature of the active site. Specifically, we considered several Cu-cation positions within the 6N and 9N pores of the CTF system using smaller cluster models shown in Figure 1b,c. For each adsorbate, we also evaluated various oxidation states, spin multiplicities,[59,60] and the possibility of intraframework hydrogen bonds to determine the most energetically favorable binding geometry. Although Pourbaix diagrams are commonly used to determine adsorbate coverages at varying potentials, it is critical to determine the most energetically favorable reaction cycle for the 4-electron process in order to predict ORR activity. Starting from a bare Cu cation, we considered the following possibilities for each subsequent step:

- A proton−electron transfer occurs on an existing ORR adsorbate.
- Additional ORR adsorbates bind to the Cu atom.
- A proton−electron transfer occurs on the nitrogen atoms lining the pore.
- Surrounding water molecules adsorb to the metal cation.
- Water or ORR adsorbates dissociate between Cu and nitrogen atoms in a chemical step.

By choosing the most energetically favorable possibility at each step of the reaction, a full ORR mechanism is obtained when a previous state is revisited. This corresponds to a complete 4 proton−electron cycle for ORR.

3.2. Benchmarking Computational Methods. The mechanism analysis summarized above is agnostic to the choice of the electronic structure method. However, an unsuitable electronic structure method may lead to inaccurate binding energies and result in an erroneous reaction mechanism. Specifically, GGA DFT is prone to self-interaction errors for nonmetallic systems.[61−64] A useful approach to circumvent these shortcomings is to incorporate Hartree−Fock exact exchange in the functional. We benchmarked several GGA and hybrid functionals to assess the accuracy of these DFT methods to describe Cu/CTF.

The coupled-cluster theory with triple excitations, CCSD(T), is a highly accurate single reference method, and it is commonly considered as the gold standard for computational quantum chemistry.[65−69] In this work, we employed the computationally tractable DLPNO approximation to benchmark GGA and hybrid DFT functionals.[46,70−72] Although less expensive than canonical CCSD(T), a smaller cluster shown in Figure 2a (denoted as 2-phen) was used for the DLPNO-CCSD(T) calculations for all adsorbates. Here, the carbon/nitrogen framework was constrained to prevent structural distortion, and only the adsorbate atoms were allowed to relax. The effects of cluster truncation on the binding energy of ORR adsorbates are presented in Figure S2.

We considered three common GGA functionals (PBE,[39] RPBE,[38] and BEEF−vdW[28]) and three hybrid functionals (B3LYP,[41] PBE0,[40] and HSE06[42,43]) in our analysis. PBE and RPBE are among the most common functionals used to study catalyst surfaces with DFT, and the BEEF−vdW functional predicts chemisorption energies on metallic surfaces with similar accuracy to RPBE[28] while inherently accounting for dispersion corrections. The B3LYP and PBE0 hybrid functionals have been used to describe a wide range of molecular systems and transition-metal complexes.[73−76] HSE06 differs from the PBE0 functional by adding the range-separated screening of the exact exchange. D3 dispersion corrections with BJ damping (D3(BJ))[44−46] were applied to all of the functionals except BEEF−vdW. Because *OOH, *O, *OH, and *H_2O are the most relevant adsorbates in the ORR mechanism, we benchmarked six DFT functionals to DLPNO-CCSD(T) based on the binding energies of these four species on 2-phen. The details of these calculations are reported in the Computational Methods section.

Figure 2b,c shows the binding energy of each ORR adsorbate on 2-phen calculated by DLPNO-CCSD(T) and by different functionals. For most adsorbates, GGA functionals result in stronger binding energies (by up to 1 eV) than hybrid functionals. The largest differences are seen for *O, followed by *OOH and *OH. As expected, we predict similar *H_2O binding energies using different methods.

DOI: 10.1021/acs.jpcc.8b09430
J. Phys. Chem. C 2018, 122, 29307−29318

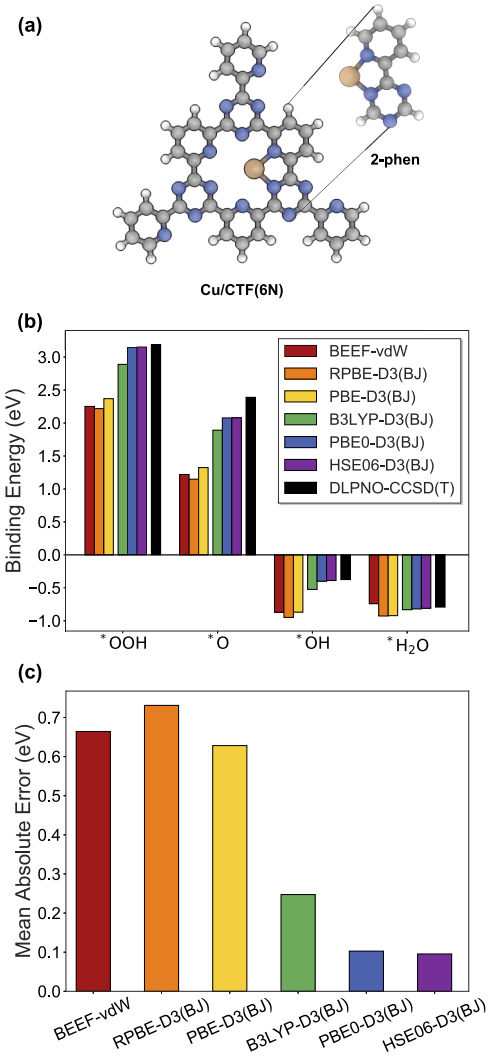

Figure 2. (a) Structure of the 2-phen truncated cluster; (b) Comparison of ORR adsorbate binding energies on 2-phen predicted by GGA and hybrids vs DLPNO-CCSD(T); (c) MAE between DLPNO-CCSD(T) and each DFT method on 2-phen.

Overall, the binding energies predicted by PBE0 and HSE06 hybrid functionals align most closely with the DLPNO-CCSD(T) benchmark with a mean absolute error (MAE) of 0.1 eV. The largest deviations are seen for *O ($MAE_{HSE06,PBE0}$ = 0.3 eV), which is not typically involved in the rate-limiting step of the ORR mechanism.[77] These results indicate that hybrid functionals, namely, HSE06 and PBE0, describe the electronic structure of this system more accurately than GGA functionals (MAE_{GGA} = 0.6−0.7 eV). Although unsurprising because of the localized electron density of isolated transition-metal sites in single-atom catalysts (Figure S4), these results highlight the large errors associated with using semi-local GGA functionals for such systems. A number of benchmarking studies for similar mono-nuclear copper-containing complexes in literature also indicate that hybrid functionals better represent various properties of these systems.[78,79] It is important to note that additional considerations such as relativistic effects and the multireference wave function character may play a role in the Cu/CTF system, but they are beyond the scope of this study.[80] Nevertheless, our results suggest that the blind use of GGA functionals to describe single-atom catalysts may produce inaccurate results.

Encouraged by the HSE06 and PBE0 results, we also explored the effect of adding a Hubbard correction (U), which is often implemented with GGA functionals to reduce the self-interaction error of DFT.[81] Figure S5 compares HSE06 with PBE + U with a U value of 5 eV applied to the 3d electrons of copper atoms based on previous literature reports of copper oxide surfaces.[82] Although the predicted errors of up to 0.5 eV for PBE + U are smaller than those for GGAs, our results indicate that careful evaluation of PBE + U is necessary for different adsorbates because the deviations may not be systematic.

3.3. Secondary Solvation Effects. Using binding energies calculated with the accurate HSE06-D3(BJ) functional, the previous primary mechanism analysis predicts a theoretical limiting potential of 0.5 V_{RHE} for Cu/CTF, where adsorption of the weak-binding *OOH intermediate limits the activity of the catalyst. However, previous studies have established that solvation effects can significantly affect the predicted ORR activity for typical transition-metal catalysts by stabilizing reaction intermediates.[83]

As the electronic structure of these nontraditional single-atom materials is very different from metal electrocatalysts, we compared the charges and the electrostatic potential surface for Cu/CTF and for Cu(111). Our analysis reveals that ORR adsorbates, especially *O, on Cu/CTF exhibit greater polarization and more direct exposure to solvent (Figure 3a−d), indicating that solvation effects are likely to be larger than widely studied metal catalysts.[84−86]

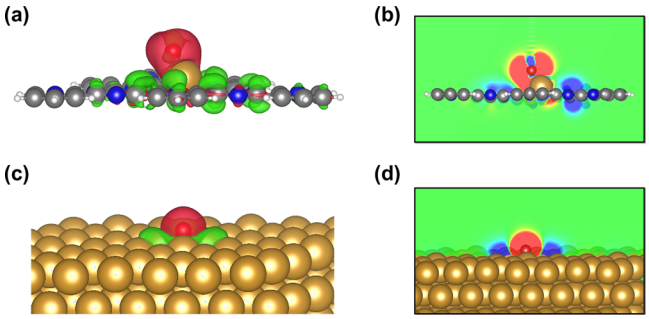

Figure 3. Charge density difference isosurfaces (±0.001 electrons/Bohr^3) and sections for the *O adsorbate on (a,b) Cu/CTF(6N) and (c,d) Cu(111) surface relative to the bare framework and isolated *O adsorbate. Red isosurfaces correspond to charges accumulation, and green isosurfaces correspond to charge depletion.

Computational strategies for describing solvation effects for metals, oxides, molecules, and biomolecules have been widely studied.[83,87−90] To provide context for our results, it is useful to summarize the popular approaches relevant to single-atom catalysts. Although some reports do not include solvation contributions, a popular approach is to define a standard correction based on hydrogen bond strengths or solvation studies of well-known metal surfaces, such as Pt(111).[91−93] Because of the ease of transferability across similar catalysts, this approach has proven useful for large-scale screening studies.[94]

Alternatively, implicit solvent models (e.g. polarizable continuum model and conductor-like screening model) are also often used to describe solvation for single-atom heterogeneous catalysts or similar homogeneous systems with marginal increase in the computational costs.[60,95−99] The performance of these methods for predicting solvation energies

DOI: 10.1021/acs.jpcc.8b09430
J. Phys. Chem. C 2018, 122, 29307−29318

generally depends on the modeling functions used and their parametrization. Although implicit solvent models have proved very useful for estimating solvation energies of organic molecules,[100−102] the transferability of this approach to a strongly polarized Cu/CTF system is not clear. Moreover, implicit approaches may not fully capture dynamic interactions between the framework and solvent molecules, such as hydrogen bonding,[103] which are important for ORR intermediates.

As an alternative to implicit solvent approaches, explicit solvent models offer the possibility to theoretically capture all important interactions between solutes and individual water molecules. However, explicit approaches require sampling thousands of solvent configurations, resulting in significant computational expense. Previous explicit solvent studies on various catalyst surfaces have employed a minima hopping algorithm[104] to find energetically favorable water structures.[86,105−108] Although minima hopping is readily applied to metal surfaces, this method is prohibitively expensive for Cu/CTF. Note that the minima hopping approach uses optimized water structures to estimate solvation; it is possible that water structures at finite temperatures may lead to differences in calculated solvation energies.

One approach to address these issues is to obtain ensemble averages of solvation energies by sampling a large number of water configurations at relevant temperatures.[109] The high computational cost of sufficient ensemble sampling (often 10^4 to 10^6 water configurations for converged values) often necessitates the use of classical MD or MC simulations based on force fields. For instance, approaches such as TI have been used extensively to predict solvation free energies from classical simulations.[110−113] Other hybrid approaches that combine quantum mechanical methods, classical explicit molecules, and implicit solvents[114,115] have also been used.

As illustrated in Figure 4, we investigated several methods to describe solvation for Cu/CTF, including both implicit and explicit solvent approaches. To obtain a consistent metric to evaluate these methods, we compared the solvation energy of each ORR intermediate on Cu/CTF. For the Cu/CTF(6N) active site, certain adsorbates, such as *OOH and *H_2O, can donate hydrogen bonds to either water molecules in the solvent or nitrogen atoms in the CTF framework, which results in significant changes in the adsorbate geometries in the presence of an aqueous solvent. Therefore, we probed orientations where these species donate hydrogen bonds to the framework (e.g. OOH_{down}) as well as those where the adsorbates donate hydrogen bonds to the water solvent (e.g. OOH_{up}).

The following sections discuss various solvation methods considered in this study: (a) implicit solvent models, (b) ab-initio cluster-continuum models, and (c) TI using DFT-derived force fields. Each of these solvation metrics were evaluated for single adsorbates on the Cu/CTF(6N) active site.

3.3.1. Implicit Solvent. We applied the VASPsol package[116,117] to evaluate solvation energies predicted by an implicit solvent. While our benchmarking results indicate that HSE06-D3(BJ) best describes the binding energies of ORR adsorbates on the Cu/CTF system, the dispersion-corrected RPBE functional has been shown to replicate experimental properties of liquid water.[118] Here, we evaluated both the HSE06-D3(BJ) and RPBE-D3(BJ) functionals to calculate the solvation-corrected binding energies. The results did not exhibit significant functional dependence (≤0.2 eV), which is consistent with previous reports.[119]

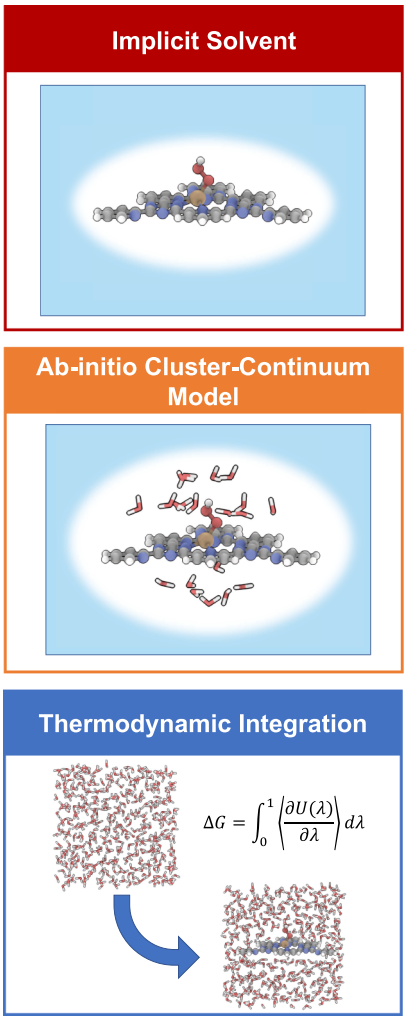

Figure 4. Schematics of solvation metrics considered in this study.

Figure 5a displays solvation energies evaluated by various metrics for each ORR intermediate species relative to *H_2O_{down} on the Cu/CTF(6N) active site. The implicit solvent results indicate that the *O adsorbate exhibits the largest solvation energy of 0.7 eV. It is important to note that this value is significantly greater than that of transition-metal surfaces, where *O solvation energy is often negligibly small.[2,120]

Although implicit solvents provide fast and inexpensive starting points for evaluating solvation effects, it is unclear whether they fully capture the interactions of ORR adsorbates for Cu/CTF. Models that include explicit water atoms provide, in principle, a more comprehensive bottom-up strategy to describe solvation, which can be used to benchmark other methods.

3.3.2. Ab Initio Cluster-Continuum Model. Purely explicit water simulations require many configurations to sufficiently sample phase space, but it is possible to reduce the number of configurations and water molecules required to converge solvation energies by surrounding a cluster containing an explicit water shell with an implicit solvent, as illustrated in Figure 4. This cluster-continuum approach[121] allows system-specific adsorbate/water interactions to be captured by an explicit solvent while reducing convergence requirements with an implicit solvent.

We explored this possibility by carving a solvation shell of 20 water molecules from 100 configurations predicted by MC

DOI: 10.1021/acs.jpcc.8b09430
J. Phys. Chem. C 2018, 122, 29307−29318

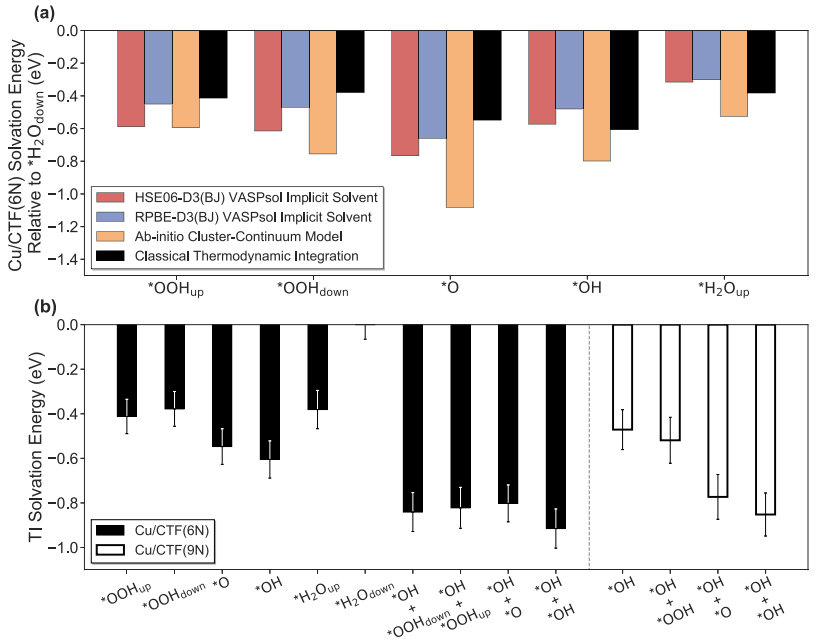

Figure 5. (a) Mean solvation energies for each ORR adsorbate relative to $*H_2O_{down}$ on Cu/CTF(6N) computed from VASPsol implicit solvent, ab-initio cluster-continuum models, and classical TI. (b) Classical TI solvation energies for all relevant adsorbate configurations on Cu/CTF(6N) and Cu/CTF(9N) relative to the bare Cu active site.

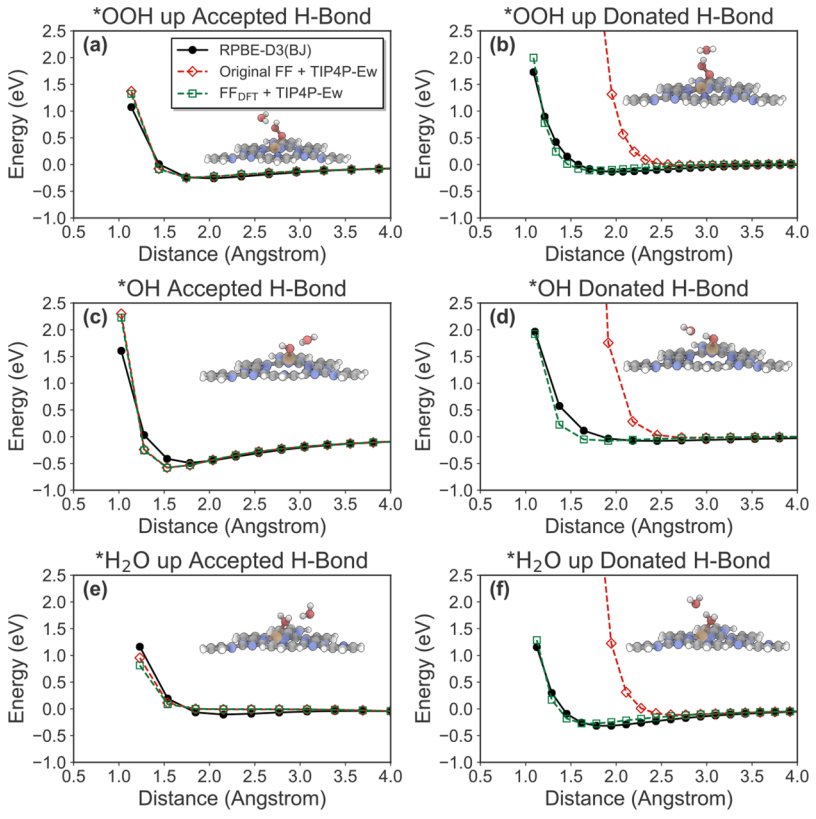

Figure 6. Potential energy curves for the interaction between single water molecules and Cu/CTF with adsorbed *OOH (a,b), *OH (c,d), and $*H_2O$ (e,f). Potential energy curves were sampled for adsorbates both accepting hydrogen bonds from water (a,c,e) and donating hydrogen bonds (b,d,f).

simulations for each adsorbate and modeling these frozen 20 water systems with the RPBE-D3(BJ) functional and the VASPsol implicit solvent (see the Computational Methods section for details). The average solvation energy for each adsorbate, $\langle \Delta E_{ads,solv} \rangle$, was calculated relative to a reference adsorbate (E_{ref}) according to eq 6.

$$\langle \Delta E_{ads,solv} \rangle = \langle E_{ads,solvated} \rangle - \langle E_{ref,solvated} \rangle - (E_{ads,vacuum} - E_{ref,vacuum}) \quad (6)$$

The solvation energies for ORR adsorbates on Cu/CTF(6N) shown in Figure 5a indicate that the cluster-continuum method

DOI: 10.1021/acs.jpcc.8b09430
J. Phys. Chem. C 2018, 122, 29307−29318

predicts greater relative solvent stabilization than an implicit model for *O and several other adsorbates (0.1−0.5 eV). One limitation of the cluster-continuum model is its incomplete description of entropic differences between adsorbate configurations due to the frozen explicit water shell. For the Cu/CTF system, the neglected configurational entropy of explicit water molecules can lead to overestimated relative solvation energies for strongly interacting adsorbates, such as *O.

To circumvent this issue, we can tune the number of water molecules included in the frozen explicit solvation shell[121] or utilize alternative free-energy methods that describe both water/solvent interactions and entropic contributions arising from solvent configurational changes. We explored the latter approach by employing TI with a classical force field to describe adsorbate solvation energies on Cu/CTF. A major drawback of classical force fields is the poor description of the system energetics relative to DFT. We address this concern by performing TI using a DFT-derived force field, as discussed below.

3.3.3. Classical TI Using DFT-Derived Force Fields. 3.3.3.1. Classical Force Field Fitting. Explicit solvation approaches require thorough sampling of the configurational phase space of water molecules surrounding a solute. Given the considerable computational expense of this endeavor via ab-initio methods, we performed classical MC simulations to obtain an ensemble of Boltzmann-sampled water configurations for each ORR adsorbate on Cu/CTF. A generic UFF/TraPPE force field was used for these simulations at 300 K,[54] and water molecules were represented by a modified TIP4P-Ew model.[122] The Cu/CTF framework and the adsorbates were frozen in these MC simulations for simplicity. Additional details are included in the Computational Methods section.

Previous reports have demonstrated that fitting force field parameters to ab-initio calculations improve agreement between classical simulations and experimentally measured material properties.[123,124] To obtain reliable water configurations and solvation energies from classical simulations, we established the accuracy of our force field by fitting adsorbate/solvent interactions to DFT using the RPBE-D3(BJ) functional. Using DFT-derived electrostatic potentials, we used the density-derived electrostatic and chemical charge (DDEC) partitioning scheme[125] to assign point charges to each atom. Pairwise vdW interactions were modeled using the LJ potential, which has two tunable parameters (ϵ and σ in eq 7) defined by the force field. To ensure that the force field accurately captured adsorbate/solvent interactions, we performed potential energy scans (PES) for hydrogen bond formation between ORR adsorbates and water molecules using the classical force field and DFT with the RPBE-D3(BJ) functional. The corresponding LJ parameters in the force field were fitted to match the DFT-derived PES. Figure 6a−f shows the water/adsorbate PES for hydrogen bonds accepted by ORR adsorbates and donated to single water molecules. The classical and DFT-derived PES for accepted hydrogen bonds align closely, but the off-the-shelf force field fails to describe hydrogen bonds donated by adsorbates to solvent water molecules. We employed a simple optimization scheme to fit the interactions between adsorbate hydrogen and water oxygen atoms using a least squares fitting procedure for force field and DFT energetics. The optimized value of ϵ for the interaction between adsorbate hydrogens and water oxygens is 0 K, which indicates that this interaction is dominated by electrostatic contributions. As shown in Figure 6a−f, the DFT-derived force field (FF_{DFT}, green) accurately describes H bond interactions compared to RPBE-D3(BJ) (black). Other validation tests for FF_{DFT} performance using additional water molecules are presented in Figures S6 and S7, which indicate that relative water/adsorbate interactions described by FF_{DFT} are comparable to RPBE-D3(BJ) results.

$$U_{vdW} = 4\epsilon\left(\left(\frac{\sigma}{r}\right)^{12} - \left(\frac{\sigma}{r}\right)^{6}\right) \tag{7}$$

3.3.3.2. Thermodynamic Integration. In TI, the free energy difference (ΔG) between two states is defined according to eq 8, where U is the potential energy of the system, and λ is a coupling parameter that spans from 0 to 1 in order to relate the initial and final states via a thermodynamic path. To describe solvation energy, this parameter is varied in specified increments to remove electrostatic and vdW interactions between a solute and solvent. In this work, classical MC simulations using FF_{DFT} were performed at each λ value along each leg of the thermodynamic path to obtain the expectation value of $\partial U/\partial\lambda$. These values were numerically integrated with respect to λ to calculate the free energy difference between two states. Additional details about TI implementation are provided in the Computational Methods.

$$\Delta G = \int_0^1 \left\langle \frac{\partial U}{\partial \lambda} \right\rangle d\lambda \tag{8}$$

Relative solvation energies from TI are reported in Figure 5a,b. Of the individual adsorbates on the 6N site, *O and *OH exhibit the largest solvation energies. This result aligns with our analysis of radial distribution functions between adsorbate oxygens and water hydrogens in Figure S8, which show closer solvation shells for these species compared to other ORR adsorbates.

Classical descriptions of solvation energy offer the ability to partition the total interaction energy into vdW and electrostatic components. For each adsorbate on the CTF system, vdW interactions account for less than 0.1 eV of the solvation energy. As a result, electrostatic contributions dominate solvation energetics, which may be a result of the cationic nature of the Cu atom in the framework.

Of the solvation metrics investigated in this study, TI using FF_{DFT} provides the most reliable solvation energies by describing adsorbate/solvent interactions explicitly and accounting for the free energy differences between adsorbates. TI was therefore performed on all of the relevant adsorbate configurations on both the 6N and 9N active sites and used in subsequent analysis in this work.

We note that implicit solvation using the RPBE-D3(BJ) functional agrees with TI within approximately 0.2 eV for most of the individual ORR adsorbates. The agreement between the VASPsol implicit solvation method and explicit TI for several adsorbates motivates the future use of such techniques to efficiently estimate solvation effects on CTF or similar inorganic catalysts. However, implicit solvent methods should be benchmarked when possible to avoid significant inaccuracies, and accurate simulations of activation barriers often require explicit approaches when transition states involve solvent molecules.

It is important to note that while our benchmarking studies of DFT methods indicate that GGA functionals overbind ORR adsorbates compared to more accurate hybrid functionals, solvent interactions also lead to stronger binding energies by stabilizing adsorbates. We suggest that favorable error

DOI: 10.1021/acs.jpcc.8b09430
J. Phys. Chem. C 2018, 122, 29307−29318

cancellation between primary and secondary effects may partially account for the success of GGA functionals in predicting ORR activity of single-atom catalysts in other reports.

3.4. ORR Activity Prediction. In this study, the goal of benchmarking computational methods to describe single-atom catalysts is to accurately predict the catalytic activity of these systems for ORR. It is therefore useful to consider the predicted ORR activity of Cu/CTF using benchmarked computational methods in the context of experimentally observed results. Although a direct comparison of theoretical current−voltage performance requires kinetic analysis,[7,126] a popular strategy is to compare the theoretical overpotential of Cu/CTF to a widely studied Pt/C catalyst. Specifically, previous theoretical studies have shown that the thermodynamic limiting potential for Pt/C determined by DFT is approximately 0.8 V_{RHE},[126] and experimental reports indicate that Cu/CTF exhibits a 0.2 V decrease in the onset potential compared to Pt/C.[33] We therefore expect the theoretical limiting potential of Cu/CTF to be 0.8 V_{RHE} − 0.2 V_{RHE} = 0.6 V_{RHE}.

To predict the ORR activity of the Cu/CTF system, we applied our findings from DFT benchmarking studies, which identified HSE06-D3(BJ) as an appropriate method, and TI-derived solvation energies to the methodology outlined in Section 3.1 to perform the ORR mechanism analysis. The free energy diagrams in Figure 7a,b show the most favorable ORR pathway predicted by the HSE06-D3(BJ) functional for both the 6N and 9N active sites on Cu/CTF before and after including solvation effects by TI. The initial and final states of the most favorable 4-electron ORR cycle in each case are boxed.

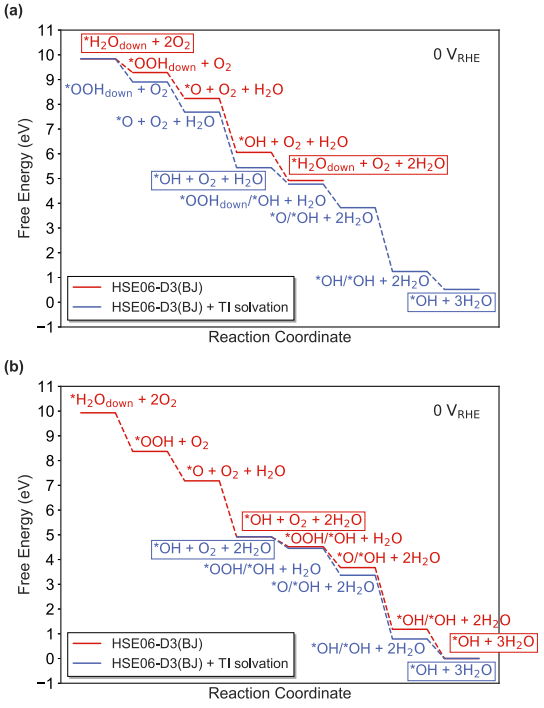

Figure 7. ORR free energy diagrams at 0 V_{RHE} evaluated using the HSE06-D3(BJ) functional and TI solvation free energies on the (a) Cu/CTF(6N) and (b) Cu/CTF(9N) active sites, where the dashed lines represent proton−electron transfers.

Without solvation corrections, single ORR adsorbates bind to the 6N site, but the 9N site adsorbs both *OH and a second adsorbate to undergo ORR. The predicted limiting reaction step is *OOH adsorption, and the theoretical ORR limiting potential is 0.6 V_{RHE} for Cu/CTF(6N) and 0.4 V_{RHE} for Cu/CTF(9N). After applying TI solvation free energies for each adsorbate, we find that the reaction mechanism and predicted theoretical limiting potential are largely unchanged for the Cu/CTF(9N) site. This is because the solvation energies of the adsorbate configurations involved in the rate-determining step (adsorption of *OOH in the presence of *OH) are similar to that of the reference species, which is *OH in this case.

In contrast, there are significant changes in both the predicted ORR mechanism and limiting potential for the 6N site after incorporating solvation effects. Specifically, adsorption of two ORR adsorbates becomes energetically favorable due to solvent stabilization, which translates to increased adsorbate coverage. The adsorption of *OOH in the presence of *OH is the rate-limiting step, and the resulting theoretical limiting potential for this pathway is 0.7 V_{RHE}. Our results from HSE06-D3(BJ) with solvation for the Cu/CTF(6N) active site indeed fall within range of the estimated experimental value.

Based on our analysis of primary and secondary effects on the Cu/CTF system, we find that appropriate descriptions of the electronic structure of single-atom catalysts and solvation effects are crucial to describe the catalytic activity of these materials. Although the most appropriate electronic structure and solvation methods may vary for other single-atom catalyst motifs, we provide a broad framework for evaluating various contributions to the ORR activity of these systems. We suggest that extending these methods to other single-atom catalysts and understanding the role of exact exchange in overall catalytic activity trends are potential directions for future study.

In addition to the primary and secondary analysis, one may also consider tertiary effects, such as anharmonic contributions to the free energy of the system[127] or the coupling of the framework and solvent entropies. Other tertiary effects may include the implications of adding support materials (i.e. graphene, carbon nanoparticles, and metal surfaces) or kinetic contributions based on reaction barriers. Although these considerations are beyond the scope of this work, they offer potential directions for future work on single-atom systems.

4. CONCLUSIONS

In this work, we have developed a methodology to guide theoretical treatment of single-atom catalysts by specifically considering Cu/CTF as a case study. Benchmarking various DFT methods to DLPNO-CCSD(T) reveals that hybrid functionals, namely, PBE0-D3(BJ) and HSE06-D3(BJ), best describe the electronic structure of Cu/CTF. By evaluating adsorbate/solvent interactions with TI and other methods, we also find that secondary effects (such as solvation) play significant roles in the predicted ORR pathway and activity of Cu/CTF. The theoretically predicted activity of Cu/CTF described by hybrid functionals combined with solvation effects aligns with estimated ORR limiting potentials based on experimental studies. Our findings also suggest that the success of commonly used GGA functionals in predicting the activity of single-atom catalysts may result from error cancellation between an accurate description of the electronic structure and solvation effects. We expect that this theoretical assessment will lead to a more complete understanding of the catalytic behavior of this promising novel material class.

DOI: 10.1021/acs.jpcc.8b09430
J. Phys. Chem. C 2018, 122, 29307−29318

■ ASSOCIATED CONTENT

Supporting Information

The Supporting Information is available free of charge on the ACS Publications website at DOI: 10.1021/acs.jpcc.8b09430.

Free energy corrections for ORR adsorbates, basis set convergence and DFT functional benchmarking figures for CTF, tables of charges and spin states for relevant configurations, force field versus DFT comparison figures, radial distribution functions for explicit water molecules surrounding ORR adsorbates, and the Pourbaix diagram for CTF stability (PDF)

■ AUTHOR INFORMATION

Corresponding Authors

*E-mail: arkulkarni@ucdavis.edu (A.R.K).
*E-mail: jkno@dtu.dk (J.K.N.).

ORCID

Anjli M. Patel: 0000-0002-0590-7619
Samira Siahrostami: 0000-0002-1192-4634
Michal Bajdich: 0000-0003-1168-8616

Notes

The authors declare no competing financial interest.

■ ACKNOWLEDGMENTS

The authors thank the Toyota Research Institute (TRI) for support through the SUNCAT Center for Interface Science and Catalysis and the National Science Foundation Graduate Research Fellowship Program (NSF GRFP). This work used the Extreme Science and Engineering Discovery Environment (XSEDE), which is supported by National Science Foundation grant number ACI-1548562.

■ REFERENCES

(1) Sui, S.; Wang, X.; Zhou, X.; Su, Y.; Riffat, S.; Liu, C.-j. A comprehensive review of Pt electrocatalysts for the oxygen reduction reaction: Nanostructure, activity, mechanism and carbon support in PEM fuel cells. *J. Mater. Chem. A* **2017**, *5*, 1808−1825.

(2) Nørskov, J. K.; Rossmeisl, J.; Logadottir, A.; Lindqvist, L.; Kitchin, J. R.; Bligaard, T.; Jónsson, H. Origin of the overpotential for oxygen reduction at a fuel-cell cathode. *J. Phys. Chem. B* **2004**, *108*, 17886−17892.

(3) Seh, Z. W.; Kibsgaard, J.; Dickens, C. F.; Chorkendorff, I.; Nørskov, J. K.; Jaramillo, T. F. Combining theory and experiment in electrocatalysis: Insights into materials design. *Science* **2017**, *355*, No. eaad4998.

(4) Xia, W.; Mahmood, A.; Liang, Z.; Zou, R.; Guo, S. Earth-Abundant Nanomaterials for Oxygen Reduction. *Angew. Chem., Int. Ed.* **2016**, *55*, 2650−2676.

(5) Gewirth, A. A.; Varnell, J. A.; DiAscro, A. M. Nonprecious Metal Catalysts for Oxygen Reduction in Heterogeneous Aqueous Systems. *Chem. Rev.* **2018**, *118*, 2313−2339.

(6) Wu, H. B.; Lou, X. W. Metal-organic frameworks and their derived materials for electrochemical energy storage and conversion: Promises and challenges. *Sci. Adv.* **2017**, *3*, No. eaap9252.

(7) Kulkarni, A.; Siahrostami, S.; Patel, A.; Nørskov, J. K. Understanding Catalytic Activity Trends in the Oxygen Reduction Reaction. *Chem. Rev.* **2018**, *118*, 2302−2312.

(8) Montoya, J. H.; Seitz, L. C.; Chakthranont, P.; Vojvodic, A.; Jaramillo, T. F.; Nørskov, J. K. Materials for solar fuels and chemicals. *Nat. Mater.* **2017**, *16*, 70−81.

(9) Wang, Y.; Zhang, W.; Deng, D.; Bao, X. Two-dimensional materials confining single atoms for catalysis. *Chin. J. Catal.* **2017**, *38*, 1443−1453.

(10) Liang, S.; Hao, C.; Shi, Y. The Power of Single-Atom Catalysis. *ChemCatChem* **2015**, *7*, 2559−2567.

(11) Yin, P.; Yao, T.; Wu, Y.; Zheng, L.; Lin, Y.; Liu, W.; Ju, H.; Zhu, J.; Hong, X.; Deng, Z.; et al. Single Cobalt Atoms with Precise N-Coordination as Superior Oxygen Reduction Reaction Catalysts. *Angew. Chem., Int. Ed.* **2016**, *55*, 10800−10805.

(12) Cheng, Q.; Yang, L.; Zou, L.; Zou, Z.; Chen, C.; Hu, Z.; Yang, H. Single cobalt atom and N codoped carbon nanofibers as highly durable electrocatalyst for oxygen reduction reaction. *ACS Catal.* **2017**, *7*, 6864−6871.

(13) Cao, R.; Thapa, R.; Kim, H.; Xu, X.; Gyu Kim, M.; Li, Q.; Park, N.; Liu, M.; Cho, J. Promotion of oxygen reduction by a bio-inspired tethered iron phthalocyanine carbon nanotube-based catalyst. *Nat. Commun.* **2013**, *4*, ncomms3076.

(14) Zhu, C.; Fu, S.; Shi, Q.; Du, D.; Lin, Y. Single-Atom Electrocatalysts. *Angew. Chem., Int. Ed.* **2017**, *56*, 13944−13960.

(15) Back, S.; Kulkarni, A. R.; Siahrostami, S. Single Metal Atoms Anchored in Two-Dimensional Materials: Bifunctional Catalysts for Fuel Cell Applications. *ChemCatChem* **2018**, *10*, 3034−3039.

(16) Siahrostami, S.; Li, G.-L.; Nørskov, J. K.; Studt, F. Trends in Adsorption Energies of the Oxygenated Species on Single Platinum Atom Embedded in Carbon Nanotubes. *Catal. Lett.* **2017**, *147*, 2689−2696.

(17) Zagal, J. H.; Koper, M. T. M. Reactivity Descriptors for the Activity of Molecular MN4 Catalysts for the Oxygen Reduction Reaction. *Angew. Chem., Int. Ed.* **2016**, *55*, 14510−14521.

(18) Chen, X.; Yu, L.; Wang, S.; Deng, D.; Bao, X. Highly active and stable single iron site confined in graphene nanosheets for oxygen reduction reaction. *Nano Energy* **2017**, *32*, 353−358.

(19) Liu, Q.; Zhang, J. Graphene Supported Co-g-C3N4 as a Novel Metal-Macrocyclic Electrocatalyst for the Oxygen Reduction Reaction in Fuel Cells. *Langmuir* **2013**, *29*, 3821−3828.

(20) Zheng, Y.; Jiao, Y.; Zhu, Y.; Cai, Q.; Vasileff, A.; Li, L. H.; Han, Y.; Chen, Y.; Qiao, S.-Z. Molecule-Level g-C3N4 Coordinated Transition Metals as a New Class of Electrocatalysts for Oxygen Electrode Reactions. *J. Am. Chem. Soc.* **2017**, *139*, 3336−3339.

(21) Zhang, C.; Sha, J.; Fei, H.; Liu, M.; Yazdi, S.; Zhang, J.; Zhong, Q.; Zou, X.; Zhao, N.; Yu, H.; et al. Single-Atomic Ruthenium Catalytic Sites on Nitrogen-Doped Graphene for Oxygen Reduction Reaction in Acidic Medium. *ACS Nano* **2017**, *11*, 6930−6941.

(22) Liu, J.; Jiao, M.; Lu, L.; Barkholtz, H. M.; Li, Y.; Wang, Y.; Jiang, L.; Wu, Z.; Liu, D.-j.; Zhuang, L.; et al. High performance platinum single atom electrocatalyst for oxygen reduction reaction. *Nat. Commun.* **2017**, *8*, 15938.

(23) Li, F.; Han, G.-F.; Noh, H.-J.; Kim, S.-J.; Lu, Y.; Jeong, H. Y.; Fu, Z.; Baek, J.-B. Boosting oxygen reduction catalysis with abundant copper single atom active sites. *Energy Environ. Sci.* **2018**, *11*, 2263−2269.

(24) Zhang, X.; Chen, A.; Zhang, Z.; Jiao, M.; Zhou, Z. Transition metal anchored C2N monolayers as efficient bifunctional electrocatalysts for hydrogen and oxygen evolution reactions. *J. Mater. Chem. A* **2018**, *6*, 11446−11452.

(25) Yang, L.; Cheng, D.; Xu, H.; Zeng, X.; Wan, X.; Shui, J.; Xiang, Z.; Cao, D. Unveiling the high-activity origin of single-atom iron catalysts for oxygen reduction reaction. *Proc. Natl. Acad. Sci. U.S.A.* **2018**, *115*, 6626−6631.

(26) Calle-Vallejo, F.; Loffreda, D.; Koper, M. T. M.; Sautet, P. Introducing structural sensitivity into adsorption-energy scaling relations by means of coordination numbers. *Nat. Chem.* **2015**, *7*, 403−410.

(27) de Morais, R. F.; Sautet, P.; Loffreda, D.; Franco, A. A. A multiscale theoretical methodology for the calculation of electrochemical observables from ab initio data: Application to the oxygen reduction reaction in a Pt(111)-based polymer electrolyte membrane fuel cell. *Electrochim. Acta* **2011**, *56*, 10842−10856.

(28) Wellendorff, J.; Lundgaard, K. T.; Møgelhøj, A.; Petzold, V.; Landis, D. D.; Nørskov, J. K.; Bligaard, T.; Jacobsen, K. W. Density functionals for surface science: Exchange-correlation model develop-

DOI: 10.1021/acs.jpcc.8b09430
J. Phys. Chem. C 2018, 122, 29307−29318

ment with Bayesian error estimation. *Phys. Rev. B: Condens. Matter Mater. Phys.* **2012**, *85*, 235149.
(29) Wellendorff, J.; Silbaugh, T. L.; Garcia-Pintos, D.; Nørskov, J. K.; Bligaard, T.; Studt, F.; Campbell, C. T. A benchmark database for adsorption bond energies to transition metal surfaces and comparison to selected DFT functionals. *Surf. Sci.* **2015**, *640*, 36−44.
(30) Sharada, S. M.; Bligaard, T.; Luntz, A. C.; Kroes, G.-J.; Nørskov, J. K. SBH10: A Benchmark Database of Barrier Heights on Transition Metal Surfaces. *J. Phys. Chem. C* **2017**, *121*, 19807−19815.
(31) Kuhn, P.; Antonietti, M.; Thomas, A. Porous, covalent triazine-based frameworks prepared by ionothermal synthesis. *Angew. Chem., Int. Ed.* **2008**, *47*, 3450−3453.
(32) Ding, S.-Y.; Wang, W. Covalent organic frameworks (COFs): from design to applications. *Chem. Soc. Rev.* **2013**, *42*, 548−568.
(33) Iwase, K.; Yoshioka, T.; Nakanishi, S.; Hashimoto, K.; Kamiya, K. Copper-Modified Covalent Triazine Frameworks as Non-Noble-Metal Electrocatalysts for Oxygen Reduction. *Angew. Chem., Int. Ed.* **2015**, *54*, 11068−11072.
(34) Kamiya, K.; Kamai, R.; Hashimoto, K.; Nakanishi, S. Platinum-modified covalent triazine frameworks hybridized with carbon nanoparticles as methanol-tolerant oxygen reduction electrocatalysts. *Nat. Commun.* **2014**, *5*, 5040.
(35) Iwase, K.; Kamiya, K.; Miyayama, M.; Hashimoto, K.; Nakanishi, S. Sulfur-Linked Covalent Triazine Frameworks Doped with Coordinatively Unsaturated Cu(I) as Electrocatalysts for Oxygen Reduction. *ChemElectroChem* **2018**, *5*, 805−810.
(36) Kresse, G.; Furthmüller, J. Efficient iterative schemes forab initiototal-energy calculations using a plane-wave basis set. *Phys. Rev. B: Condens. Matter Mater. Phys.* **1996**, *54*, 11169−11186.
(37) Joubert, D. From ultrasoft pseudopotentials to the projector augmented-wave method. *Phys. Rev. B: Condens. Matter Mater. Phys.* **1999**, *59*, 1758−1775.
(38) Hammer, B.; Hansen, L. B.; Nørskov, J. K. Improved adsorption energetics within density-functional theory using revised Perdew-Burke-Ernzerhof functionals. *Phys. Rev. B: Condens. Matter Mater. Phys.* **1999**, *59*, 7413−7421.
(39) Perdew, J. P.; Burke, K.; Ernzerhof, M. Generalized gradient approximation made simple. *Phys. Rev. Lett.* **1996**, *77*, 3865−3868.
(40) Adamo, C.; Barone, V. Toward reliable density functional methods without adjustable parameters: The PBE0 model. *J. Chem. Phys.* **1999**, *110*, 6158−6170.
(41) Stephens, P. J.; Devlin, F. J.; Chabalowski, C. F.; Frisch, M. J. Ab Initio Calculation of Vibrational Absorption and Circular Dichroism Spectra Using Density Functional Force Fields. *J. Phys. Chem.* **1994**, *98*, 11623−11627.
(42) Heyd, J.; Scuseria, G. E.; Ernzerhof, M. Hybrid functionals based on a screened Coulomb potential. *J. Chem. Phys.* **2003**, *118*, 8207−8215.
(43) Krukau, A. V.; Vydrov, O. A.; Izmaylov, A. F.; Scuseria, G. E. Influence of the exchange screening parameter on the performance of screened hybrid functionals. *J. Chem. Phys.* **2006**, *125*, 224106.
(44) Grimme, S.; Ehrlich, S.; Goerigk, L. Effect of the damping function in dispersion corrected density functional theory. *J. Comput. Chem.* **2011**, *32*, 1456−1465.
(45) Grimme, S.; Antony, J.; Ehrlich, S.; Krieg, H. A consistent and accurate ab initio parametrization of density functional dispersion correction (DFT-D) for the 94 elements H-Pu. *J. Chem. Phys.* **2010**, *132*, 154104.
(46) Smith, D. G. A.; Burns, L. A.; Patkowski, K.; Sherrill, C. D. Revised Damping Parameters for the D3 Dispersion Correction to Density Functional Theory. *J. Phys. Chem. Lett.* **2016**, *7*, 2197−2203.
(47) Neese, F. *ORCA*, version 4.0; Max-Planck Institut für Chemische Energiekonversion: Mülheim a. d. Ruhr, Germany, 2010.
(48) Valeev, E. F. Libint: A library for the evaluation of molecular integrals of many-body operators over Gaussian functions. http://libint.valeyev.net/ (accessed May 23, 2017).
(49) Neese, F.; Solomon, E. I. Calculation of Zero-Field Splittings, g-Values, and the Relativistic Nephelauxetic Effect in Transition Metal Complexes. Application to High-Spin Ferric Complexes. *Inorg. Chem.* **1998**, *37*, 6568−6582.
(50) Neese, F. Importance of Direct Spin−Spin Coupling and Spin-Flip Excitations for the Zero-Field Splittings of Transition Metal Complexes: A Case Study. *J. Am. Chem. Soc.* **2006**, *128*, 10213−10222.
(51) Kendall, R. A.; Dunning, T. H.; Harrison, R. J. Electron affinities of the first-row atoms revisited. Systematic basis sets and wave functions. *J. Chem. Phys.* **1992**, *96*, 6796−6806.
(52) Balabanov, N. B.; Peterson, K. A. Systematically convergent basis sets for transition metals. I. All-electron correlation consistent basis sets for the 3d elements Sc-Zn. *J. Chem. Phys.* **2005**, *123*, 064107.
(53) Balabanov, N. B.; Peterson, K. A. Basis set limit electronic excitation energies, ionization potentials, and electron affinities for the 3d transition metal atoms: Coupled cluster and multireference methods. *J. Chem. Phys.* **2006**, *125*, 074110.
(54) Dubbeldam, D.; Calero, S.; Ellis, D. E.; Snurr, R. Q. RASPA: Molecular simulation software for adsorption and diffusion in flexible nanoporous materials. *Mol. Simul.* **2015**, *42*, 81−101.
(55) Beutler, T. C.; Mark, A. E.; van Schaik, R. C.; Gerber, P. R.; van Gunsteren, W. F. Avoiding singularities and numerical instabilities in free energy calculations based on molecular simulations. *Chem. Phys. Lett.* **1994**, *222*, 529−539.
(56) Mruzik, M. R.; Abraham, F. F.; Schreiber, D. E.; Pound, G. M. A Monte Carlo study of ion-water clusters. *J. Chem. Phys.* **1976**, *64*, 481−491.
(57) Mezei, M.; Beveridge, D. L. Free Energy Simulations. *Ann. N.Y. Acad. Sci.* **1986**, *482*, 1−23.
(58) Mezei, M. The finite difference thermodynamic integration, tested on calculating the hydration free energy difference between acetone and dimethylamine in water. *J. Chem. Phys.* **1987**, *86*, 7084−7088.
(59) Orellana, W. Catalytic properties of transition metal-N4 moieties in graphene for the oxygen reduction reaction: Evidence of spin-dependent mechanisms. *J. Phys. Chem. C* **2013**, *117*, 9812−9818.
(60) McClure, J. P.; Borodin, O.; Olguin, M.; Chu, D.; Fedkiw, P. S. Sensitivity of Density Functional Theory Methodology for Oxygen Reduction Reaction Predictions on Fe-N4-Containing Graphitic Clusters. *J. Phys. Chem. C* **2016**, *120*, 28545−28562.
(61) Sham, L. J.; Schlüter, M. Density-functional theory of the energy gap. *Phys. Rev. Lett.* **1983**, *51*, 1888−1891.
(62) Perdew, J. P.; Levy, M. Physical content of the exact kohn-sham orbital energies: Band gaps and derivative discontinuities. *Phys. Rev. Lett.* **1983**, *51*, 1884−1887.
(63) Seidl, A.; Görling, A.; Vogl, P.; Majewski, J. A.; Levy, M. Generalized Kohn-Sham schemes and the band-gap problem. *Phys. Rev. B: Condens. Matter Mater. Phys.* **1996**, *53*, 3764−3774.
(64) Perdew, J. P. Density functional theory and the band gap problem. *Int. J. Quantum Chem.* **2009**, *28*, 497−523.
(65) Raghavachari, K.; Trucks, G. W.; Pople, J. A.; Head-Gordon, M. A fifth-order perturbation comparison of electron correlation theories. *Chem. Phys. Lett.* **1989**, *157*, 479−483.
(66) Lee, T. J.; Scuseria, G. E. *Quantum Mechanical Electronic Structure Calculations with Chemical Accuracy*; Springer Netherlands: Dordrecht, 1995; pp 47−108.
(67) Scuseria, G. E.; Lee, T. J. Comparison of coupled-cluster methods which include the effects of connected triple excitations. *J. Chem. Phys.* **1990**, *93*, 5851−5855.
(68) Ghosh, S.; Verma, P.; Cramer, C. J.; Gagliardi, L.; Truhlar, D. G. Combining Wave Function Methods with Density Functional Theory for Excited States. *Chem. Rev.* **2018**, *118*, 7249−7292.
(69) Goodpaster, J. D.; Barnes, T. A.; Manby, F. R.; Miller, T. F. Density functional theory embedding for correlated wavefunctions: Improved methods for open-shell systems and transition metal complexes. *J. Chem. Phys.* **2012**, *137*, 224113.
(70) Riplinger, C.; Sandhoefer, B.; Hansen, A.; Neese, F. Natural triple excitations in local coupled cluster calculations with pair natural orbitals. *J. Chem. Phys.* **2013**, *139*, 134101.

DOI: 10.1021/acs.jpcc.8b09430
J. Phys. Chem. C 2018, 122, 29307−29318

(71) Liakos, D. G.; Sparta, M.; Kesharwani, M. K.; Martin, J. M. L.; Neese, F. Exploring the accuracy limits of local pair natural orbital coupled-cluster theory. *J. Chem. Theory Comput.* **2015**, *11*, 1525−1539.
(72) Minenkov, Y.; Chermak, E.; Cavallo, L. Accuracy of DLPNO-CCSD(T) Method for Noncovalent Bond Dissociation Enthalpies from Coinage Metal Cation Complexes. *J. Chem. Theory Comput.* **2015**, *11*, 4664−4676.
(73) Tirado-Rives, J.; Jorgensen, W. L. Performance of B3LYP density functional methods for a large set of organic molecules. *J. Chem. Theory Comput.* **2008**, *4*, 297−306.
(74) Bühl, M.; Kabrede, H. Geometries of Transition-Metal Complexes from Density-Functional Theory. *J. Chem. Theory Comput.* **2006**, *2*, 1282−1290.
(75) Zhou, X.-P.; Li, D.; Zheng, S.-L.; Zhang, X.; Wu, T. Cu(I) or Cu(I)−Cu(II) Mixed-Valence Complexes of 2,4,6-Tri(2-pyridyl)-1,3,5-triazine: Syntheses, Structures, and Theoretical Study of the Hydrolytic Reaction Mechanism. *Inorg. Chem.* **2006**, *45*, 7119−7125.
(76) Coskun, D.; Jerome, S. V.; Friesner, R. A. Evaluation of the Performance of the B3LYP, PBE0, and M06 DFT Functionals, and DBLOC-Corrected Versions, in the Calculation of Redox Potentials and Spin Splittings for Transition Metal Containing Systems. *J. Chem. Theory Comput.* **2016**, *12*, 1121−1128.
(77) Viswanathan, V.; Hansen, H. A.; Rossmeisl, J.; Nørskov, J. K. Universality in oxygen reduction electrocatalysis on metal surfaces. *ACS Catal.* **2012**, *2*, 1654−1660.
(78) Weymuth, T.; Couzijn, E. P. A.; Chen, P.; Reiher, M. New benchmark set of transition-metal coordination reactions for the assessment of density functionals. *J. Chem. Theory Comput.* **2014**, *10*, 3092−3103.
(79) Siegbahn, P. E. M. The performance of hybrid DFT for mechanisms involving transition metal complexes in enzymes. *JBIC, J. Biol. Inorg. Chem.* **2006**, *11*, 695−701.
(80) Liakos, D. G.; Neese, F. Interplay of Correlation and Relativistic Effects in Correlated Calculations on Transition-Metal Complexes: The (Cu2O2)2+Core Revisited. *J. Chem. Theory Comput.* **2011**, *7*, 1511−1523.
(81) Anisimov, V. I.; Zaanen, J.; Andersen, O. K. Band theory and Mott insulators: Hubbard U instead of Stoner I. *Phys. Rev. B: Condens. Matter Mater. Phys.* **1991**, *44*, 943−954.
(82) Bhola, K.; Varghese, J. J.; Dapeng, L.; Liu, Y.; Mushrif, S. H. Influence of Hubbard U parameter in simulating adsorption and reactivity on CuO: Combined theoretical and experimental study. *J. Phys. Chem. C* **2017**, *121*, 21343−21353.
(83) Karlberg, G. S. Adsorption trends for water, hydroxyl, oxygen, and hydrogen on transition-metal and platinum-skin surfaces. *Phys. Rev. B: Condens. Matter Mater. Phys.* **2006**, *74*, 153414.
(84) Sha, Y.; Yu, T. H.; Liu, Y.; Merinov, B. V.; Goddard, W. A. Theoretical Study of Solvent Effects on the Platinum-Catalyzed Oxygen Reduction Reaction. *J. Phys. Chem. Lett.* **2010**, *1*, 856−861.
(85) Yu, L.; Pan, X.; Cao, X.; Hu, P.; Bao, X. Oxygen reduction reaction mechanism on nitrogen-doped graphene: A density functional theory study. *J. Catal.* **2011**, *282*, 183−190.
(86) Reda, M.; Hansen, H. A.; Vegge, T. DFT study of stabilization effects on N-doped graphene for ORR catalysis. *Catal. Today* **2018**, *312*, 118−125.
(87) Hansen, N.; van Gunsteren, W. F. Practical Aspects of Free-Energy Calculations: A Review. *J. Chem. Theory Comput.* **2014**, *10*, 2632−2647.
(88) Ytreberg, F. M.; Swendsen, R. H.; Zuckerman, D. M. Comparison of free energy methods for molecular systems. *J. Chem. Phys.* **2006**, *125*, 184114.
(89) Ren, P.; Chun, J.; Thomas, D. G.; Schnieders, M. J.; Marucho, M.; Zhang, J.; Baker, N. A. Biomolecular electrostatics and solvation: a computational perspective. *Q. Rev. Biophys.* **2012**, *45*, 427−491.
(90) Rossmeisl, J.; Greeley, J.; Karlberg, G. *Fuel Cell Catalysis*; John Wiley & Sons, Inc.: Hoboken, NJ, USA, pp 57−92.
(91) Calle-Vallejo, F.; Martínez, J. I.; García-Lastra, J. M.; Abad, E.; Koper, M. T. M. Oxygen reduction and evolution at single-metal active sites: Comparison between functionalized graphitic materials and protoporphyrins. *Surf. Sci.* **2013**, *607*, 47−53.
(92) Baran, J. D.; Grönbeck, H.; Hellman, A. Analysis of porphyrines as catalysts for electrochemical reduction of O2 and oxidation of H2O. *J. Am. Chem. Soc.* **2014**, *136*, 1320−1326.
(93) Kattel, S.; Atanassov, P.; Kiefer, B. Catalytic activity of Co-Nx/C electrocatalysts for oxygen reduction reaction: a density functional theory study. *Phys. Chem. Chem. Phys.* **2013**, *15*, 148−153.
(94) Calle-Vallejo, F.; Martínez, J. I.; Rossmeisl, J. Density functional studies of functionalized graphitic materials with late transition metals for oxygen reduction reactions. *Phys. Chem. Chem. Phys.* **2011**, *13*, 15639.
(95) Sperger, T.; Sanhueza, I. A.; Kalvet, I.; Schoenebeck, F. Computational Studies of Synthetically Relevant Homogeneous Organometallic Catalysis Involving Ni, Pd, Ir, and Rh: An Overview of Commonly Employed DFT Methods and Mechanistic Insights. *Chem. Rev.* **2015**, *115*, 9532−9586.
(96) Calle-Vallejo, F.; Krabbe, A.; García-Lastra, J. M. How covalence breaks adsorption-energy scaling relations and solvation restores them. *Chem. Sci.* **2017**, *8*, 124−130.
(97) Mussell, S.; Choudhury, P. Density Functional Theory Study of Iron Phthalocyanine Porous Layer Deposited on Graphene Substrate: A Pt-Free Electrocatalyst for Hydrogen Fuel Cells. *J. Phys. Chem. C* **2016**, *120*, 5384−5391.
(98) Ringe, S.; Oberhofer, H.; Hille, C.; Matera, S.; Reuter, K. Function-Space-Based Solution Scheme for the Size-Modified Poisson-Boltzmann Equation in Full-Potential DFT. *J. Chem. Theory Comput.* **2016**, *12*, 4052−4066.
(99) Goodpaster, J. D.; Bell, A. T.; Head-Gordon, M. Identification of Possible Pathways for C-C Bond Formation during Electrochemical Reduction of CO2: New Theoretical Insights from an Improved Electrochemical Model. *J. Phys. Chem. Lett.* **2016**, *7*, 1471−1477.
(100) Gunceler, D.; Letchworth-Weaver, K.; Sundararaman, R.; Schwarz, K. A.; Arias, T. A. The importance of nonlinear fluid response in joint density-functional theory studies of battery systems. *Modell. Simul. Mater. Sci. Eng.* **2013**, *21*, 074005.
(101) Andreussi, O.; Dabo, I.; Marzari, N. Revised self-consistent continuum solvation in electronic-structure calculations. *J. Chem. Phys.* **2012**, *136*, 064102.
(102) Tomasi, J.; Mennucci, B.; Cammi, R. Quantum Mechanical Continuum Solvation Models. *Chem. Rev.* **2005**, *105*, 2999−3094.
(103) Tan, C.; Yang, L.; Luo, R. How Well Does Poisson−Boltzmann Implicit Solvent Agree with Explicit Solvent? A Quantitative Analysis. *J. Phys. Chem. B* **2006**, *110*, 18680−18687.
(104) Goedecker, S. Minima hopping: An efficient search method for the global minimum of the potential energy surface of complex molecular systems. *J. Chem. Phys.* **2004**, *120*, 9911−9917.
(105) Gauthier, J. A.; Dickens, C. F.; Chen, L. D.; Doyle, A. D.; Nørskov, J. K. Solvation Effects for Oxygen Evolution Reaction Catalysis on IrO2(110). *J. Phys. Chem. C* **2017**, *121*, 11455−11463.
(106) Montoya, J. H.; Shi, C.; Chan, K.; Nørskov, J. K. Theoretical Insights into a CO Dimerization Mechanism in CO2 Electroreduction. *J. Phys. Chem. Lett.* **2015**, *6*, 2032−2037.
(107) Kirk, C.; Chen, L. D.; Siahrostami, S.; Karamad, M.; Bajdich, M.; Voss, J.; Nørskov, J. K.; Chan, K. Theoretical Investigations of the Electrochemical Reduction of CO on Single Metal Atoms Embedded in Graphene. *ACS Cent. Sci.* **2017**, *3*, 1286−1293.
(108) Shi, C.; Chan, K.; Yoo, J. S.; Nørskov, J. K. Barriers of Electrochemical CO2 Reduction on Transition Metals. *Org. Process Res. Dev.* **2016**, *20*, 1424−1430.
(109) Schnur, S.; Groß, A. Properties of metal-water interfaces studied from first principles. *New J. Phys.* **2009**, *11*, 125003.
(110) Kirkwood, J. G. Statistical Mechanics of Fluid Mixtures. *J. Chem. Phys.* **1935**, *3*, 300−313.
(111) Steinbrecher, T.; Joung, I.; Case, D. A. Soft-core potentials in thermodynamic integration: Comparing one- and two-step transformations. *J. Comput. Chem.* **2011**, *32*, 3253−3263.
(112) Martins, S. A.; Sousa, S. F.; Ramos, M. J.; Fernandes, P. A. Prediction of solvation free energies with thermodynamic integration

DOI: 10.1021/acs.jpcc.8b09430
J. Phys. Chem. C 2018, 122, 29307−29318

using the general Amber force field. *J. Chem. Theory Comput.* **2014**, *10*, 3570−3577.
(113) Kumar, S.; Rosenberg, J. M.; Bouzida, D.; Swendsen, R. H.; Kollman, P. A. The weighted histogram analysis method for free-energy calculations on biomolecules. I. The method. *J. Comput. Chem.* **1992**, *13*, 1011−1021.
(114) Iftimie, R.; Salahub, D.; Schofield, J. An efficient Monte Carlo method for calculating ab initio transition state theory reaction rates in solution. *J. Chem. Phys.* **2003**, *119*, 11285−11297.
(115) Stecher, T.; Reuter, K.; Oberhofer, H. First-Principles Free-Energy Barriers for Photoelectrochemical Surface Reactions: Proton Abstraction at TiO2(110). *Phys. Rev. Lett.* **2016**, *117*, 276001.
(116) Mathew, K.; Sundararaman, R.; Letchworth-Weaver, K.; Arias, T. A.; Hennig, R. G. Implicit solvation model for density-functional study of nanocrystal surfaces and reaction pathways. *J. Chem. Phys.* **2014**, *140*, 084106.
(117) Mathew, K.; Hennig, R. G. Implicit self-consistent description of electrolyte in plane-wave density-functional theory. **2016**, arXiv:1601.03346.
(118) Forster-Tonigold, K.; Groß, A. Dispersion corrected RPBE studies of liquid water. *J. Chem. Phys.* **2014**, *141*, 064501.
(119) Sinstein, M.; Scheurer, C.; Matera, S.; Blum, V.; Reuter, K.; Oberhofer, H. Efficient Implicit Solvation Method for Full Potential DFT. *J. Chem. Theory Comput.* **2017**, *13*, 5582−5603.
(120) Tripković, V.; Skúlason, E.; Siahrostami, S.; Nørskov, J. K.; Rossmeisl, J. The oxygen reduction reaction mechanism on Pt(111) from density functional theory calculations. *Electrochim. Acta* **2010**, *55*, 7975−7981.
(121) Pliego, J. R.; Riveros, J. M. The Cluster−Continuum Model for the Calculation of the Solvation Free Energy of Ionic Species. *J. Phys. Chem. A* **2001**, *105*, 7241−7247.
(122) Horn, H. W.; Swope, W. C.; Pitera, J. W.; Madura, J. D.; Dick, T. J.; Hura, G. L.; Head-Gordon, T. Development of an improved four-site water model for biomolecular simulations: TIP4P-Ew. *J. Chem. Phys.* **2004**, *120*, 9665−9678.
(123) Kulkarni, A. R.; Sholl, D. S. DFT-Derived Force Fields for Modeling Hydrocarbon Adsorption in MIL-47(V). *Langmuir* **2015**, *31*, 8453−8468.
(124) Heinen, J.; Burtch, N. C.; Walton, K. S.; Dubbeldam, D. Flexible Force Field Parameterization through Fitting on the Ab Initio-Derived Elastic Tensor. *J. Chem. Theory Comput.* **2017**, *13*, 3722−3730.
(125) Manz, T. A.; Sholl, D. S. Chemically meaningful atomic charges that reproduce the electrostatic potential in periodic and nonperiodic materials. *J. Chem. Theory Comput.* **2010**, *6*, 2455−2468.
(126) Hansen, H. A.; Rossmeisl, J.; Nørskov, J. K. Surface Pourbaix diagrams and oxygen reduction activity of Pt, Ag and Ni(111) surfaces studied by DFT. *Phys. Chem. Chem. Phys.* **2008**, *10*, 3722.
(127) Li, H.; Paolucci, C.; Schneider, W. F. Zeolite Adsorption Free Energies from ab Initio Potentials of Mean Force. *J. Chem. Theory Comput.* **2018**, *14*, 929−938.

DOI: 10.1021/acs.jpcc.8b09430
J. Phys. Chem. C 2018, 122, 29307−29318